Corrosion Resistance of Zn-Ni Alloy Films Electroplated in Alkaline Zincate Solutions Containing a Brightener

Bae, Sung Hwa
Graduate School of Engineering, Kyushu, University

Oue, Satoshi
Faculty of Engineering, Kyushu University

Taninouchi, Yu-ki
Faculty of Engineering, Kyushu University

Son, Injoon
Department of Materials Science and Metallurgy, Kyungpook National University

他

出版情報：ISIJ International. 63 (11), pp.1897-1907, 2023-11-15. 日本鉄鋼協会
バージョン：

ISIJ International, Vol. 63 (2023), No. 11, pp. 1897–1907
https://doi.org/10.2355/isijinternational.ISIJINT-2023-236

Corrosion Resistance of Zn–Ni Alloy Films Electroplated in Alkaline Zincate Solutions Containing a Brightener

Sung Hwa BAE,[1] Satoshi OUE,[2] Yu-ki TANINOUCHI,[2] Injoon SON[3] and Hiroaki NAKANO[2]*

1) Graduate School of Engineering, Kyushu University, 744, Motooka, Nishi-ku, Fukuoka-shi, 819-0395 Japan.
2) Faculty of Engineering, Kyushu University, 744, Motooka, Nishi-ku, Fukuoka-shi, 819-0395 Japan.
3) Department of Materials Science and Metallurgy, Kyungpook National University, 80 Daehak-ro, Sangyeok-dong, Buk-gu, Daegu, 41566 Korea.

(*Received on June 7, 2023; accepted on August 1, 2023; originally published in Tetsu-to-Hagané, Vol. 109, 2023, No. 4, pp. 289–300*)

Zn–Ni alloys were electroplated on a Fe plate with a thickness of 40 μm at 500 A·m^{-2} and 293 K in unagitated zincate solutions. The reaction product of epichlorohydrin and imidazole (IME) was added to the solution as a brightener at concentrations of 0–5 mL dm^{-3}. The corrosion resistance of the obtained Zn–Ni alloy films was investigated from the polarization curve in 3 mass% NaCl solution before and after the corrosion treatment (formation of corrosion products) for 48 hours. Before the corrosion treatment, the corrosion current density of plated films rarely changed, regardless of the addition of IME into the zincate solution, because the reduction reaction of dissolved oxygen rarely changed. However, in films plated from the solution containing IME, the anode reaction was suppressed, and the corrosion potential shifted toward the noble direction. The suppression of the anode reaction with an addition of IME into the plating solution is attributed to the increase in γ-phase in the plated films. After the corrosion treatment, Zn chloride hydroxide of the corrosion product uniformly formed on the surface when increasing the concentration of IME. The reduction reaction of dissolved oxygen was suppressed by increasing the concentration of IME, resulting in a decrease in corrosion current density.

KEY WORDS: electroplating; zinc-nickel alloy; corrosion; corrosion current density; corrosion potential; corrosion product; polarization curve; brightener; zincate solution; zincate.

1. Introduction

Zn–Ni alloy-electroplated steel sheets have been widely used in automotive parts, home electrical appliances, and building materials due to their superior corrosion resistance compared to that of Zn-plated steel sheets.[1–8] Zn–Ni alloy electrodeposition is generally performed in sulfate and chloride solutions, but the zincate solution is a desirable alternative for electrodeposition on small components.[9–19] In Zn–Ni alloy deposition in a zincate solution, the brightener is generally added to the solution. The relationship between the final product's appearance quality and the brightener has been studied,[20–22] but the effect of the brightener in solution on the corrosion resistance of deposited films has not been extensively studied.

Zn–Ni alloy-plated films obtained from zincate solutions containing two kinds of brighteners (polyethylene glycol and vanillin, piperonal, or coumarin) have been reported to exhibit excellent corrosion resistance in Na_2SO_4 aqueous solution and superior performance compared to a brightener-free solution.[23] Zn–Ni alloy-plated films obtained from sulfate solutions containing the condensation product of salicylaldehyde and cysteine hydrochloride[24] or vanillin and glycine[25] as brighteners are reported to improve the corrosion resistance in an environment containing Cl^- ions. However, the reported corrosion resistance was examined immediately after immersion in a solution. Thus, the corrosion resistance after corrosion products have formed on the surface of plated films is unknown.

In an environment containing Cl^- ions, the corrosion resistance of Zn–Ni alloy-plated films is greater than that of Zn-plated films. This is due to the formation of a corrosion product composed of Zn chloride hydroxide ($ZnCl_2 \cdot 4Zn(OH)_2$) which has a large film resistance.[27–29] Regarding the Zn–Ni alloy-plated films obtained from zincate solutions, the formation of Zn chloride hydroxide was reportedly promoted with brighteners in an environment containing Cl^- ions.[26] However, the effect of various brighteners on the formation of Zn chloride hydroxide, as well as the process details, are unknown.

* Corresponding author: E-mail: nakano@zaiko.kyushu-u.ac.jp

Table 1. Solution composition and electrolysis condition.

ZnO	($mol \cdot dm^{-3}$)	0.15	Current density ($A \cdot m^{-2}$)	500
$NiSO_4 \cdot 6H_2O$	($mol \cdot dm^{-3}$)	0.016	Temperature (K)	293
$N(CH_2CH_2OH)_3$	($mol \cdot dm^{-3}$)	0.34	Thickness of deposits (μm)	40
NaOH	($mol \cdot dm^{-3}$)	2.5	Cathode	Fe (1×2 cm^2)
IME	($ml \cdot dm^{-3}$)	0, 1, 3. 5	Anode	Pt (1×2 cm^2)
			Quiescent bath	

Therefore, the authors selected the epichlorohydrin and imidazole (IME) reaction product as a brightener, which is reported to have a gloss effect on Zn–Ni alloy-plated films obtained from zincate solutions.[30–33] The effect of the brightener added to the electrolysis solution on the corrosion resistance of Zn–Ni alloy-plated films was investigated. In this study, the surface of the obtained Zn–Ni alloy-plated films was corrosion treated in a NaCl aqueous solution which is a representative corrosion environment containing Cl^- ions. The corrosion resistance in 3 mass% NaCl solution was evaluated using the polarization curve before and after the corrosion treatment.

2. Experimental

Table 1 shows the composition of the zincate solution and the electrolysis conditions used for the production of Zn–Ni alloy-plated films. The electrolytic solutions were prepared by dissolving reagent-grade ZnO (0.15 $mol \cdot dm^{-3}$), $NiSO_4 \cdot 6H_2O$ (0.016 $mol \cdot dm^{-3}$), $N(CH_2CH_2OH)_3$ (0.34 $mol \cdot dm^{-3}$), and NaOH (2.5 $mol \cdot dm^{-3}$) in distilled and deionized water at room temperature. The reaction product of epichlorohydrin and imidazole (IME) was prepared as previously reported.[34,35] IME was added into an electrolytic solution in amounts of 0, 1, 3, and 5 $mL \cdot dm^{-3}$. The structural formula of IME is shown in **Fig. 1**. Electrolysis was performed using the constant current electrolysis method without stirring at a current density of 500 $A \cdot m^{-2}$ and solution temperature of 293 K. Fe was used as the substrate. The amount of electricity was fixed to obtain a film thickness of 40 μm. In this study, to evaluate the corrosion resistance of plated films only, and to prevent the effect of the substrate from impacting the results, the film thickness was set to 40 μm. The details of the produced sample material are shown in **Table 2**. The Ni content in plated films obtained with an addition of 0, 1, 3, and 5 $mL \cdot dm^{-3}$ of IME was 5.0, 3.9, 3.9, and 3.8 mass%, respectively.

The corrosion treatment was performed by immersing the samples into an oxygen-saturated 3 mass% NaCl aqueous solution at 298 K. The immersing durations were 24, 48, and 168 hours. Before and after the corrosion treatment, the corrosion resistance of the plated films was evaluated by measuring the polarization curve. The polarization curves were measured from a less noble potential than the corrosion potential (*i.e.*, in the anodic-potential direction) using the potential sweep method at 10 $mV \cdot s^{-1}$ in 3% NaCl solution at 313 K. Regarding the sample materials before the corrosion treatment, the anodic current density at a constant potential of -0.8 V was also measured to evaluate the dissolution reaction of the plated films. The standard electrode potential, E^0, of Zn and Ni is -0.76 and -0.25 V vs SHE, respectively.

Table 2. Zn–Ni films subjected to a corrosion test.

IME in plating solution ($ml \cdot dm^{-3}$)	0	1	3	5
Ni content of Zn–Ni films (mass%)	5.0	3.9	3.9	3.8
Thickness of Zn–Ni films (μm)	40			

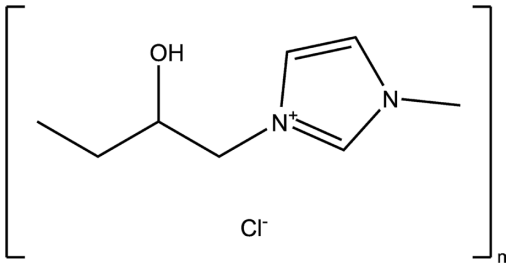

Fig. 1. Structural formula of the reaction product of epichlorohydrin and imidazole (IME).

The surface morphology of the plated films before and after the corrosion treatment was observed with scanning electron microscopy (SEM). Composition analysis of the sample after corrosion treatment was performed using energy-dispersive X-ray spectroscopy (EDX). The phase of the plated film was identified via an X-ray diffractometer (Cu-Kα, tube voltage of 40 kV, tube current of 15 mA).

To quantify the C co-deposited on the plated films before corrosion treatment, the content of C was measured using high-frequency glow discharge optical emission spectrometry (rf-GDOES). The plated films for measurement were obtained at 500 $A \cdot m^{-2}$ and 5×10^4 $C \cdot m^{-2}$ on a Cu substrate. The contents of C, Zn, Ni, and Cu in the plated films were measured by rf-GDOES under the following conditions: analysis diameter: $\phi 2$ mm, argon pressure: 600 Pa, power: 40 W, pulse frequency: 2 000 Hz, duty cycle: 0.125.

3. Results

3.1. Structure of Zn–Ni Alloy-plated Films

Figure 2 shows the appearance of the Zn–Ni alloy-plated films obtained at 500 $A \cdot m^{-2}$ from a zincate solution at 293 K containing various concentrations of IME. The plated film obtained from the IME-free solution (a) was gray and matte, while those obtained from the solutions containing 1 and 3 $mL \cdot dm^{-3}$ of IME ((b) and (c), respectively) showed some gloss. With the addition of 5 $mL \cdot dm^{-3}$ of IME (d), the plated films were silvery and significantly glossy.

Figure 3 shows the SEM images of the surface of the

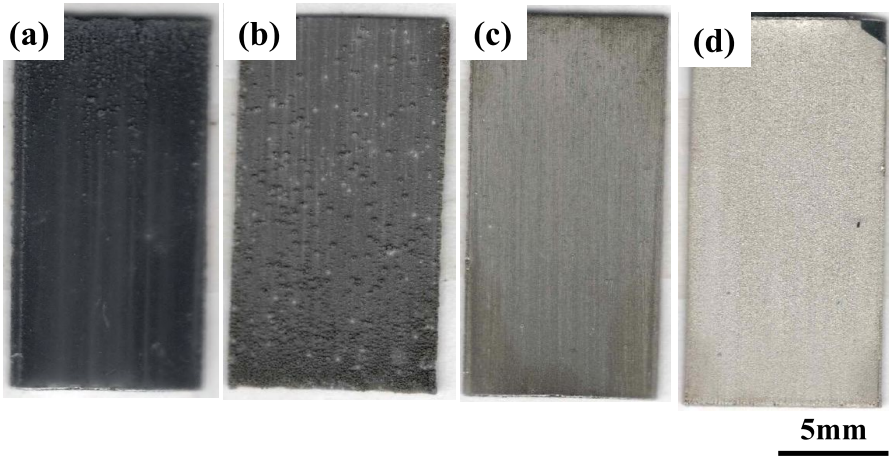

Fig. 2. Appearance of Zn–Ni alloy films deposited with a thickness of 40 μm at 500 A·m^{-2} in solutions containing various amounts of IME. [(a) IME-free, (b) IME 1 mL·dm^{-3}, (c) IME 3 mL·dm^{-3}, (d) IME 5 mL·dm^{-3}]. (Online version in color.)

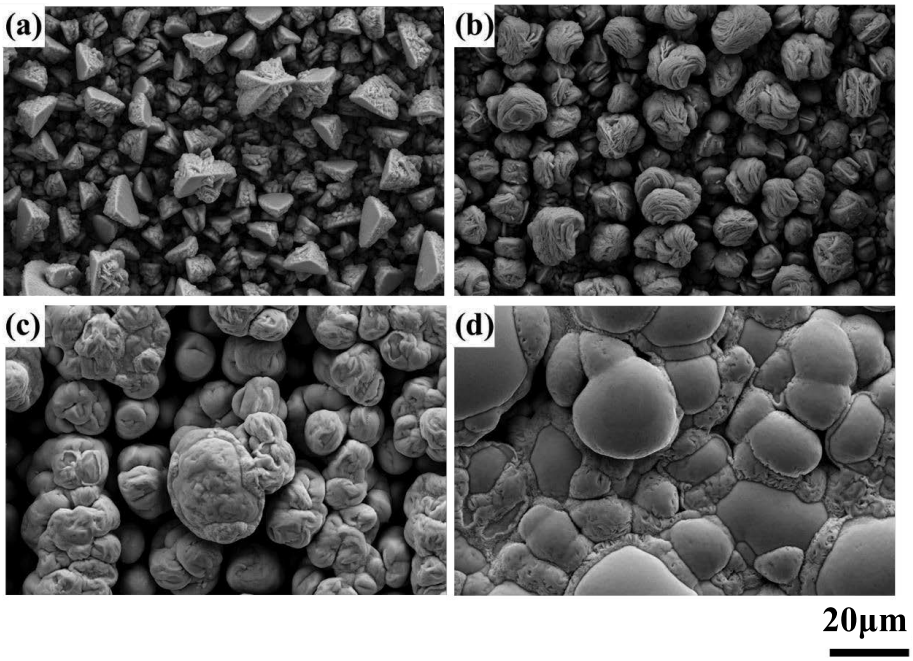

Fig. 3. SEM images of the Zn–Ni alloy films deposited with a thickness of 40 μm at 500 A·m^{-2} in solutions containing various amounts of IME. [(a) IME-free, (b) IME 1 mL·dm^{-3}, (c) IME 3 mL·dm^{-3}, (d) IME 5 mL·dm^{-3}].

Zn–Ni alloy-plated films. The plated films obtained from the IME-free solution (a) showed morphology indicating the vertical growth of the trigonal pyramid. In the plated films obtained from solutions containing 1 and 3 mL·dm^{-3} of IME ((b) and (c), respectively), the plated crystals disappeared, and roundish aggregated crystals composed of fine crystals were formed. With the addition of 5 mL·dm^{-3} of IME (d), the surface was smooth and the gaps between the aggregated crystals were coated with the plating films.

Figure 4 shows the X-ray diffraction patterns of the Zn–Ni alloy-plated films. The peak resulting from the Fe substrate was not detected, regardless of the presence of IME. Only the peaks related to the η-Zn phase, in which an Ni solid solution in Zn was formed, and the γ-phase (Ni_2Zn_{11}) of the intermetallic compounds was detected. The main peak was observed at a diffraction angle of 43.0°, but the diffraction angles of η-Zn phase and γ-phase were 43.2° and 42.8°, respectively; therefore, the η-Zn phase and γ-phase could not be identified from the main peak. However, from the diffraction peaks at 56.2° and 68.1°, γ-phase was thought to generally increase with increasing concentration of IME in the electrolytic solution.

3.2. Effect of IME on the Corrosion Resistance of Zn–Ni Alloy-plated Films

3.2.1. Corrosion Resistance Immediately after the Production of the Plated Films

Figure 5 shows the polarization curves of Zn–Ni alloy-plated films in 3 mass% NaCl solution without corrosion treatment. From the reduction current density at −1.00 V, the reduction reaction of dissolved oxygen ($O_2+2H_2O+4e^-\rightarrow 4OH^-$), which is the cathodic reaction of corrosion, was found to be nearly the same among the four types of plated films, indicating scarce changes with and

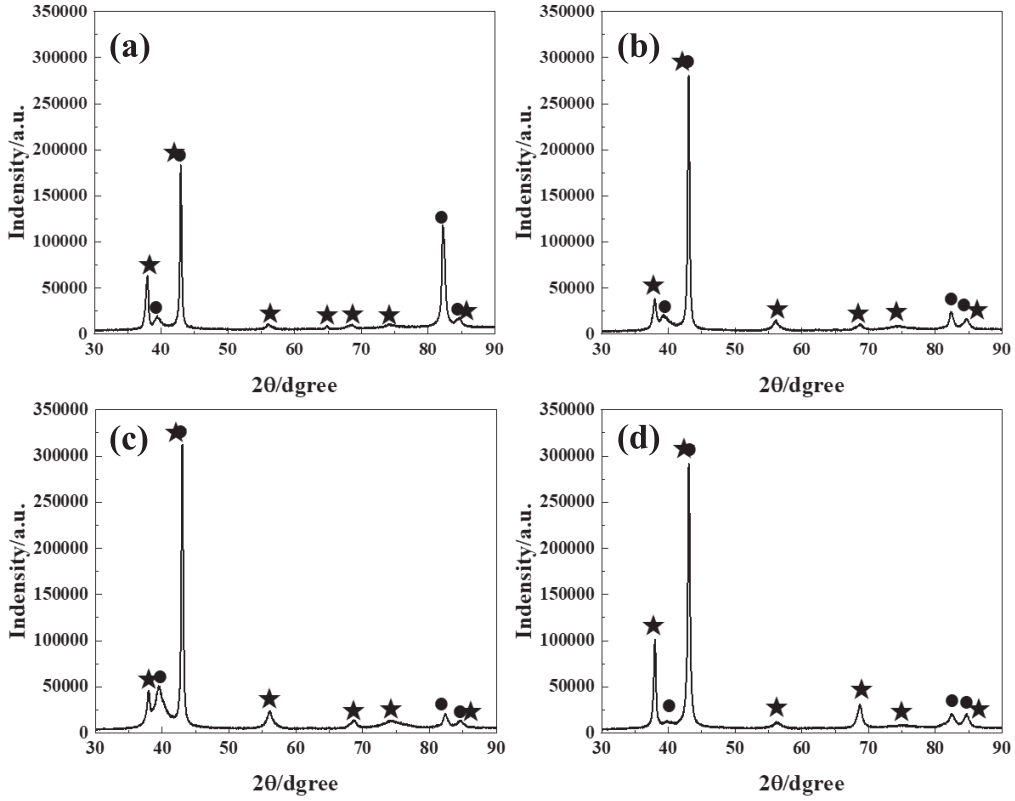

Fig. 4. X-ray diffraction patterns of the Zn–Ni alloy films deposited with a thickness of 40 μm at 500 A·m^{-2} in solutions containing various amounts of IME. [(a) IME-free, (b) IME 1 mL·dm^{-3}, (c) IME 3 mL·dm^{-3}, (d) IME 5 mL·dm^{-3}]. (● Zn[η] PDF # 87-0713 and ★ Ni_2Zn_{11}[γ] PDF # 65-5310).

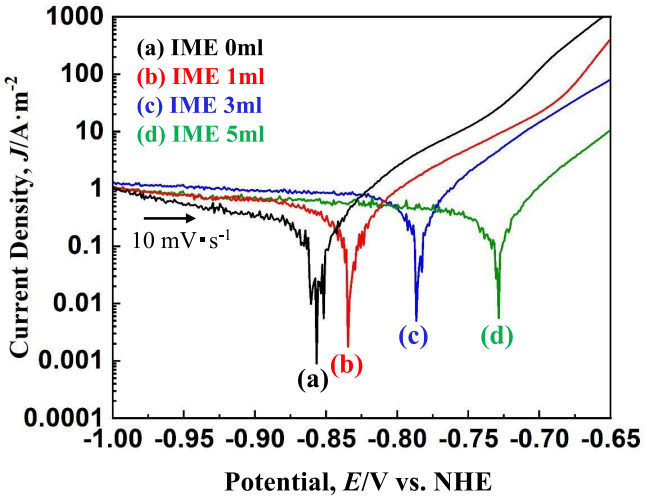

Fig. 5. Polarization curves in 3 mass% NaCl solution for corrosion product-free deposits obtained with a thicknesses of 40 μm at 500 A·m^{-2} in the solutions containing various amounts of IME. [(a) IME-free, (b) IME 1 ml · dm^{-3}, (c) IME 3 ml · dm^{-3}, (d) IME 5 ml · dm^{-3}]. (Online version in color.)

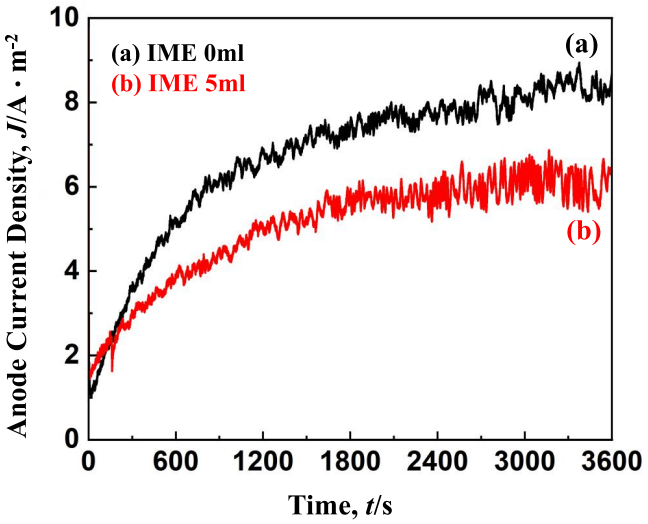

Fig. 6. Anode current density at −0.8 V in 3 mass% NaCl solution for corrosion product-free deposits obtained with a thicknesses of 40 μm at 500 A·m^{-2} in the solutions with and without IME. [(a) IME-free, (b) IME 5 ml · dm^{-3}]. (Online version in color.)

without IME. That is, the IME added into the electrolytic solution when producing the plated films negligibly affected the corrosion current density (corrosion rate) of the plated films in NaCl solution.

The corrosion potential of the plated films obtained from the IME-free solution was approximately −0.86 V, while those of alloy films obtained from the solutions containing IME were nobler. In this study, the corrosion potential was not spontaneous-potential during immersion but was defined as the potential at which the current density became zero in the polarization curve measured using LSV. Focusing on the anodic polarization curves when shifting the potential toward the anodic direction (*i.e.*, nobler than the corrosion potential), the oxidation reaction ($Zn \rightarrow Zn^{2+}+2e^-$ around corrosion potential) in the plated films obtained from solutions containing IME was suppressed. Since the oxygen

reduction of the cathodic reaction reaches the diffusion limit of oxygen and it rarely depends on the electrode potential, the change in corrosion potential is attributed to the change in the polarization of the anodic reaction.

Figure 6 shows the anodic current density at a constant potential of −0.8 V of Zn–Ni alloy-plated films in 3 mass% NaCl solution without corrosion treatment. The anodic current density, which shows the dissolution rate of Zn–Ni alloy-plated films, increased with time regardless of the presence of IME. The anodic current density decreased with increasing concentrations of IME, except for in the initial stage. The anodic current density at constant potential reflects the polarization curve of the anodic reaction, showing that the anodic reaction of corrosion is suppressed by increasing the concentration of IME from 0–5 mL·dm^{-3}. The plated films obtained in this study were composed of two phases of η-Zn phase and γ-phase (Ni_2Zn_{11}) (Fig. 4). The increase in anodic current density with time, shown in Fig. 6, is attributed to the increase in the true surface area when dissolving the plated films and an increase in η-Zn phase, which is easy to dissolve within the plated films.

3.2.2. Corrosion Resistance after Corrosion Treatment in NaCl Solution

Figure 7 shows the appearance of the Zn–Ni alloy-plated films formed at 500 A·m^{-2} and 298 K in zincate solutions containing various concentrations of IME after immersion in 3 mass% NaCl solution for 48 and 168 hours. After 48 hours of immersion, no red rust, only white rust was observed regardless of whether IME was present. The white rust was larger in plated films from the IME-free solution (a) than those from solutions containing IME ((b),(c),(d)). Any difference in white rust between the plated films obtained from solutions containing 1, 3, and 5 mL·dm^{-3} of IME was scarcely observed. However, after 168 hours of immersion, red rust was observed on all samples. The surface area of red rust was the largest on the plated films obtained from the IME-free solution (a), and decreased with increasing concentrations of IME ((f),(g),(h)).

Figure 8 shows the polarization measurement after the formation of corrosion products by immersing the Zn–Ni alloy films in 3 mass% NaCl solution for 48 hours. After 48 hours, no red rust was observed and the Fe of the substrate was not exposed (Fig. 7). The equilibrium potential of the reduction reaction of $Zn(OH)_2$ in corrosion products ($Zn(OH)_2+2e^-\rightarrow Zn+2OH^-$) is –0.85 V at a pH of 7; therefore, at a potential region less noble than −0.85 V, the reduction reaction of $Zn(OH)_2$ may occur along with the reduction of resolved oxygen. Thus, the reduction reaction of dissolved oxygen was evaluated in a potential region nobler than −0.85 V.

In plated films obtained from the solutions containing IME ((b),(c),(d)), the reduction current density of dissolved oxygen significantly decreased compared to that of the IME-free solution (a). Since the reduction reaction of dissolved oxygen is thought to reach the diffusion limit of oxygen at

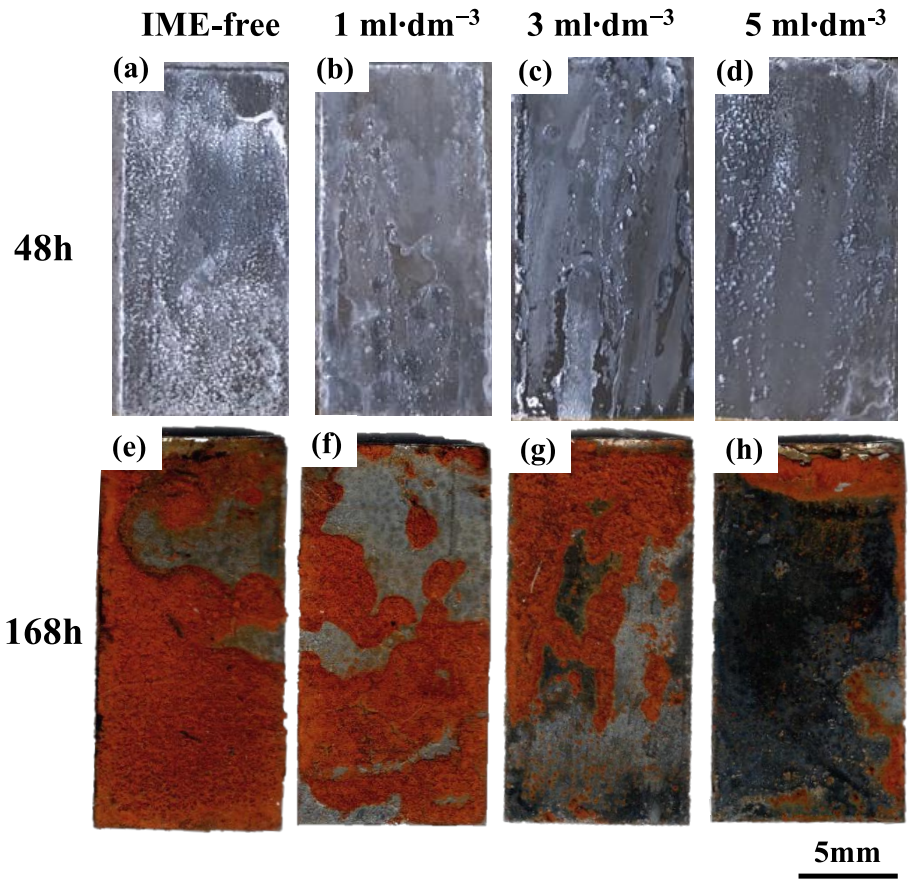

Fig. 7. Appearance after being immersed in 3 mass% NaCl solution for either 48 or 168 h of Zn–Ni alloy films deposited with a thicknesses of 40 μm at 500 A·m^{-2} in the solutions containing various amounts of IME. [(a) IME-free, 48 h, (b) IME 1 ml·dm^{-3}, 48 h, (c) IME 3 ml·dm^{-3}, 48 h, (d) IME 5 ml·dm^{-3}, 48 h, (e) IME-free, 168 h, (f) IME 1 ml·dm^{-3}, 168 h, (g) IME 3 ml·dm^{-3}, 168 h, (h) IME 5 ml·dm^{-3}, 168 h]. (Online version in color.)

the potential region measured in this study, the corrosion resistance was better in plated films obtained from the solutions containing IME. The corrosion rate was thus smaller in plated films obtained from the solutions containing IME.

The corrosion potential of plated films obtained from the IME-free solution was −0.8 V. The corrosion potential shifted toward the noble direction with increasing concentrations of IME in the electrolytic solution for plating and became −0.48 V with an addition of 5 mL·dm^{-3} of IME. The dissolution reaction of plated films, or the anodic reaction, was more suppressed with IME than without. The degree of suppression increased with increasing concentrations of IME. In the Tafel region of the anodic reaction, a linear relationship was observed in the polarization curve, and Tafel's gradient was smaller with 1 mL·dm^{-3} of IME (a) than that without IME (a), but it scarcely changed when increasing the concentration of IME ((c),(d)). The shift in the corrosion potential of plated films toward the noble direction with increasing concentrations of IME is attributed to the suppression of the anodic reaction with IME.

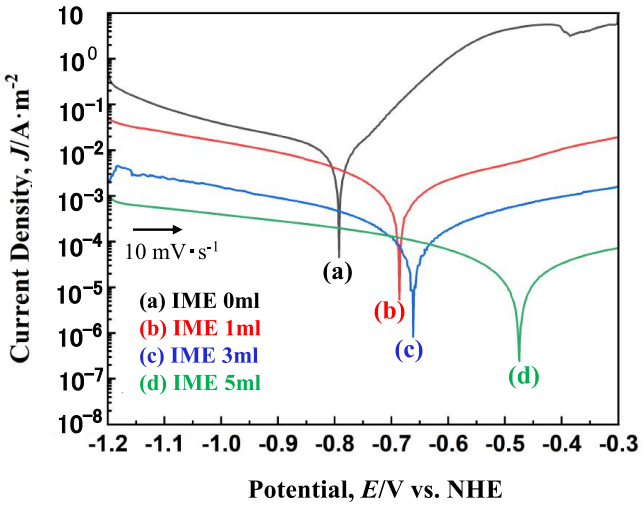

Fig. 8. Polarization curves after being immersed in 3 mass% NaCl solution for 48 h of deposits obtained with a thicknesses of 40 μm at 500 A·m^{-2} in the solutions containing various amounts of IME. [(a) IME-free, (b) IME 1 ml · dm^{-3}, (c) IME 3 ml · dm^{-3}, (d) IME 5 ml · dm^{-3}]. (Online version in color.)

Comparing the polarization curves after immersion for 48 hours in NaCl solution (Fig. 8) to that without immersion (Fig. 5), the current density for the reduction reaction of dissolved oxygen was smaller with 48 hours of immersion regardless of whether IME was added to the plating solution. That is, the corrosion rate was smaller with 48 hours of corrosion treatment. The corrosion potential was nobler with 48 hours of corrosion treatment, and the degree of shift in the corrosion potential toward the noble direction increased with increasing concentrations of IME. Comparing the anodic polarization of plated films with 48 hours of corrosion treatment obtained from solutions containing IME to that without corrosion treatment, the polarization resistance, dE/di, in the Tafel region was larger with 48 hours of corrosion treatment.

3.3. Structure of Corrosion Products after 24 and 48 Hours of Immersion in NaCl Solution

3.3.1. Analysis of Samples after 24 Hours of Corrosion Treatment

Figure 9 shows the surface SEM images of the Zn–Ni alloy films after 24 hours of immersion in 3 mass% NaCl solution. The plated films obtained from the IME-free solution (a) comprised massive crystals, which the platelet crystals aggregated, and showed a gap between the massive crystals. The center of the massive crystals was small, but the platelet crystals grew large at the edge of the massive crystals. In the plated films obtained from the solution containing 1 mL·dm^{-3} of IME (b), the thickness of

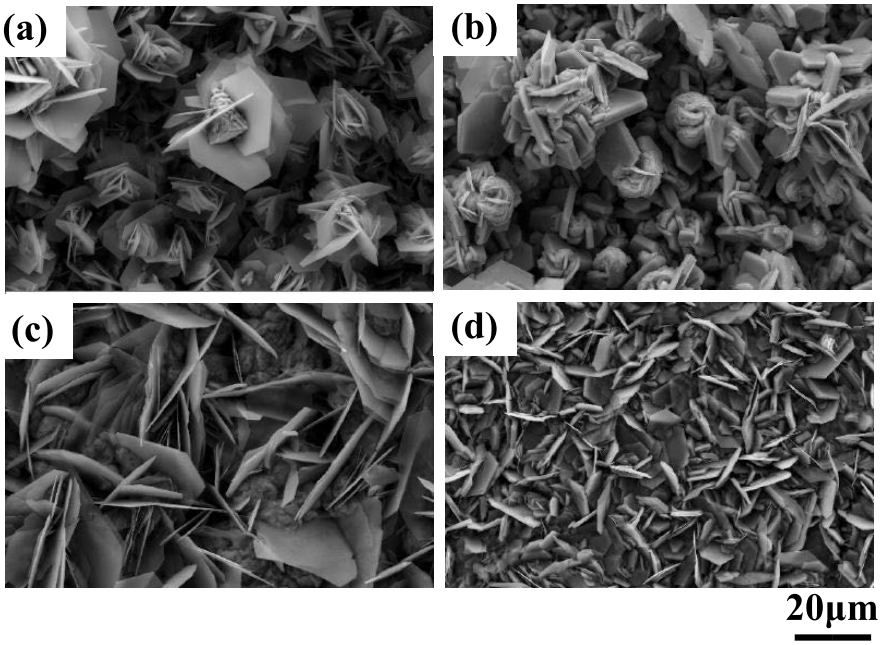

Fig. 9. SEM images after being immersed in 3 mass% NaCl solution for 24 h of deposits obtained with a thicknesses of 40 μm at 500 A·m^{-2} in the solutions containing various amounts of IME. [(a) IME-free, (b) IME 1 ml·dm^{-3}, (c) IME 3 ml·dm^{-3}, (d) IME 5 ml·dm^{-3}].

platelet crystals somewhat increased, and the gap between the massive crystals decreased. With increasing IME to 3 mL·dm^{-3} (c), the platelet crystals that largely grew inclining were mainly present. When further increasing the IME to 5 mL·dm^{-3} (d), the entire surface was uniformly covered by the platelet crystals.

Figure 10 shows the X-ray diffraction patterns of the Zn–Ni alloy-plated films after 24 hours of immersion in 3 mass% NaCl solution. In the plated films obtained from the IME-free solution (a), the main peaks resulted from the η-Zn phase and γ phase (intermetallic compound of Ni_2Zn_{11}) of the plated films, but other diffraction peaks resulting from Zn chloride hydroxide ($ZnCl_2{\cdot}4Zn(OH)_2$) and $Zn(OH)_2$ of the corrosion products of the plated films were detected. The diffraction patterns of the Zn–Ni alloy-plated films obtained from the solutions containing 1, 3, and 5 mL·dm^{-3} of IME ((b),(c),(d)) showed almost the same trend as that from the IME-free solution. Although the analysis depth of XRD differs depending on the sample, measurement wavelength, and diffraction angle, it is several hundred nm to several tens of μm for inorganic substances.[36] In this study, the outermost surface mainly comprised Zn chloride hydroxide and $Zn(OH)_2$, but Zn and Zn–Ni alloy seemed to remain on the inside. From the results mentioned above, it was found that Zn chloride hydroxide and $Zn(OH)_2$ of the corrosion products of the Zn–Ni alloy-plated films formed regardless of whether IME was added to the plating solution after 24 hours of immersion in 3 mass% NaCl solution.

Figure 11 shows the SEM images and point analysis by EDX of Zn–Ni films obtained from the IME-free solution after 24 hours of immersion in 3 mass% NaCl solution. At the center of the massive crystals ((b) in Fig. 11(a)), Zn, O, and Cl were detected, but the peak of Cl was small (Fig. 11(b)). In the area of the platelet crystals ((c) in Fig. 11(a)), which were seen at the edge of the massive crystals, Zn, O, and Cl were detected (Fig. 11(c)). When the Zn–Ni alloy-plated films were immersed in the NaCl solution, the formation of Zn chloride hydroxide ($ZnCl_2{\cdot}4Zn(OH)_2$) is expected as a corrosion product,[27–29] and Zn chloride hydroxide was reported to be the platelet crystals.[37] In this study, since the peak resulting from Zn chloride hydroxide in the X-ray diffraction patterns of the Zn–Ni alloy-plated films was detected after 24 hours of immersion in 3 mass% NaCl solution (Fig. 10), and Zn, O, and Cl were detected in the EDX analysis (Fig. 11(c)), the platelet crystals ((c) in Fig. 11(a)) which were seen at the edge of massive crystals were thought to be Zn chloride hydroxide. Since the peak of Cl was small at the center of the massive crystals ((b)

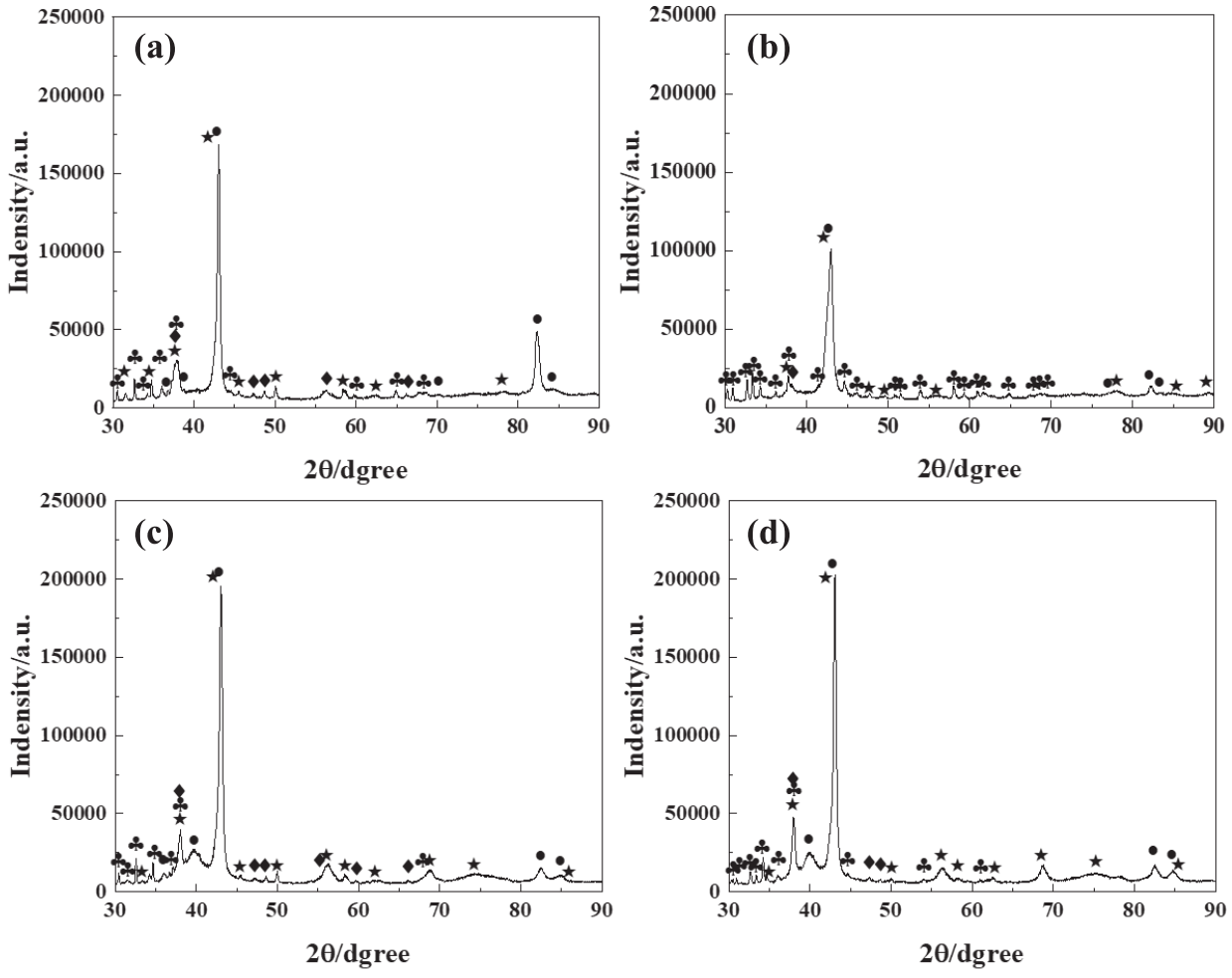

Fig. 10. X-ray diffraction patterns after being immersed in 3 mass% NaCl solution for 24 h of deposits obtained with a thicknesses of 40 μm at 500 A·m^{-2} in the solutions containing various amounts of IME. [(a) IME-free, (b) IME 1 ml·dm^{-3}, (c) IME 3 ml·dm^{-3}, (d) IME 5 ml·dm^{-3}]. (● Zn[η] PDF # 87-0713, ★ Ni_2Zn_{11}[γ] PDF # 65-5310, ♣ $ZnCl_2{\cdot}4Zn(OH)_2$ PDF # 07-0155, ♦ $Zn(OH)_2$ PDF # 41-1359).

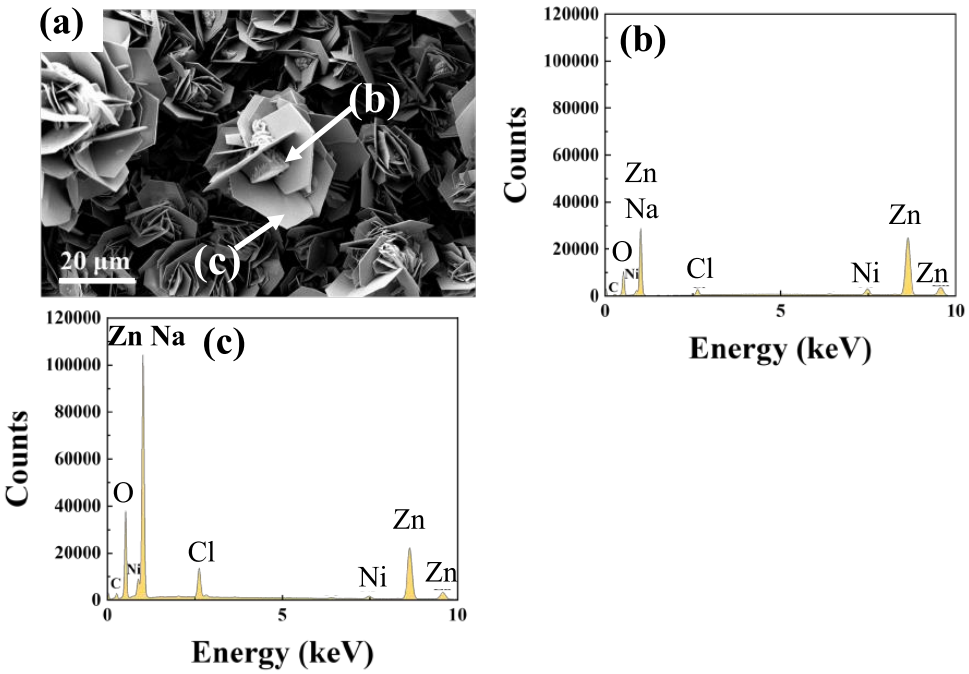

Fig. 11. SEM image and EDX spectra after being immersed in 3 mass% NaCl solution for 24 h of deposits obtained with a thicknesses of 40 μm at 500 A·m^{-2} in the IME-free solution. [(a) SEM image, (b) EDX spectrum of (b), (c) EDX spectrum of (c)]. (Online version in color.)

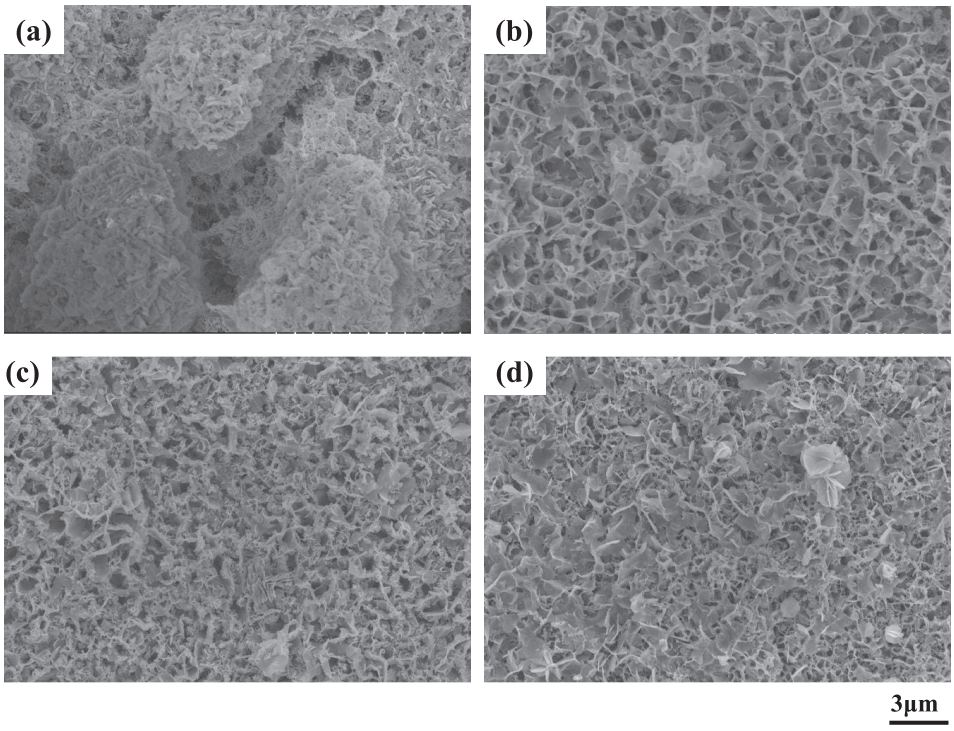

Fig. 12. SEM images after being immersed in 3 mass% NaCl solution for 48 h of deposits obtained with a thicknesses of 40 μm at 500 A·m^{-2} in the solutions containing various amounts of IME. [(a) IME-free, (b) IME 1 ml·dm^{-3}, (c) IME 3 ml·dm^{-3}, (d) IME 5 ml·dm^{-3}].

in Fig. 11(a)), the corrosion products mainly composed of $Zn(OH)_2$ were thought to be formed. From the results mentioned above, the platelet crystals (Fig. 9) seen in the Zn–Ni alloy-plated films after 24 hours of immersion in 3 mass% NaCl solution were concluded to be Zn chloride hydroxide.

3.3.2. Analysis of Samples after 48 Hours of Corrosion Treatment

Figure 12 shows the surface SEM images of the Zn–Ni alloy-plated films after 48 hours of immersion in 3 mass% NaCl solution. The plated films obtained from IME-free solution (a) comprised massive crystals, which the platelet crystals aggregated, and a large gap between the massive

crystals was seen. In the plated films obtained from the solution containing 1 mL·dm^{-3} of IME (b), the platelet crystals were formed on the entire surface and a large gap disappeared, but a large number of concavities were seen between platelet crystals. With increasing IME to 3 and 5 mL·dm^{-3} ((c) and (d), respectively), the surface coverage by the platelet crystals increased and the size of the concavities between the platelet crystals decreased. From the analysis results after 24 hours of corrosion treatment in NaCl solution, the platelet crystals (Fig. 12) which existed at the surface, were determined to be Zn chloride hydroxide.

4. Discussion

4.1. Corrosion Resistance Immediately after Production of the Plated Films

The corrosion resistance of Zn–Ni alloy-plated films obtained from the solutions containing IME is discussed below. Immediately after the production of the plated films, the corrosion current density of Zn–Ni alloy-plated films without corrosion products was almost the same regardless of whether IME was added to the plating solution (Fig. 5). The schematic diagram of the inner polarization curve of the Zn–Ni alloy-plated films considered from Fig. 5 is shown in **Fig. 13**. The corrosion rate in 3 mass% NaCl solution is controlled by the reduction reaction of dissolved oxygen, that is, by the reduction rate of oxygen. The reduction reaction of dissolved oxygen becomes a diffusion limitation of oxygen. Without corrosion products, the current density for the reduction reaction of dissolved oxygen was almost identical regardless of whether IME was added to the plating solution. As a result, the corrosion current density was not affected by the IME addition. However, the anode reaction of the Zn–Ni alloy-plated films without corrosion products (dissolution reaction of plated films) was more suppressed with plated films obtained from IME-containing solutions. As a result, the corrosion potential shifted toward the noble direction with the addition of IME.

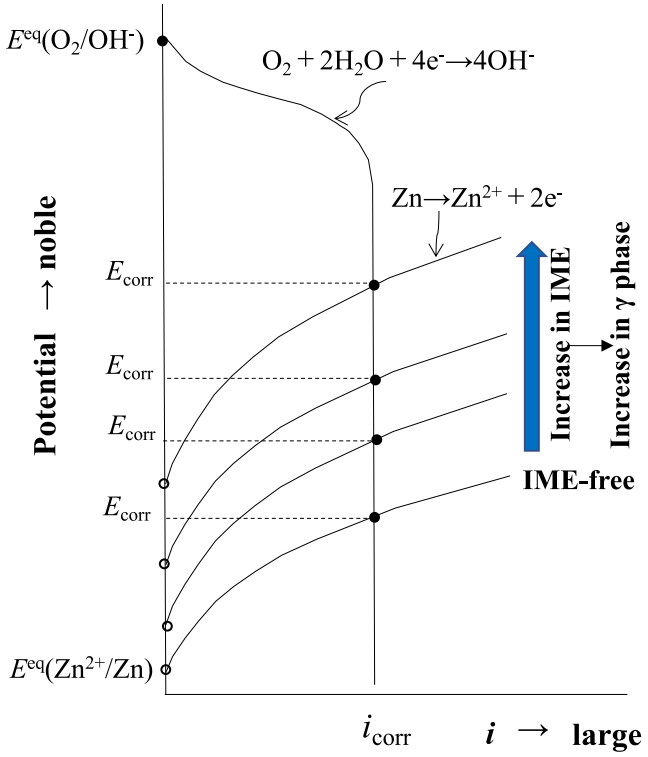

Fig. 13. Schematic diagram of internal polarization curves of corrosion product-free deposits obtained in solutions containing various amounts of IME. (Online version in color.)

When increasing the concentration of IME in the plating solution, the γ-phase (Ni_2Zn_{11}) of the intermetallic compound increased in the plated films (Fig. 4). According to the binary equilibrium diagram of the Zn–Ni system,[38] the stable region of the γ-phase at room temperature existed at a Ni content of 12.8–16.5 mass%. In electrodeposition, an increase in the overpotential for crystallization (*i.e.*, the suppression of the crystallization process) is reported to produce films of the nonequilibrium phase (high-temperature phase), similar to a rapid quenching alloy because the reduced adatoms are crystallized in a supersaturation state.[39] The brightener is reported to suppress the crystallization process in addition to the charge-transfer process.[40] In this study, since the crystallization overpotential for deposition increased with the IME of the brightener, the reduced adatoms of Zn and Ni (Zn_{ad} and Ni_{ad}) were supersaturated. Thus, the γ-phase appeared to be formed in a Ni content region different from that expected from the equilibrium diagram. The reason why the γ-phase was formed in a Ni content region lower than that of the stable γ-phase region is thought to be because the Zn formed a solid solution with the γ-phase, but the details are unknown. The γ-phase of Zn–Ni alloy-plated films is reported to be thermodynamically more stable and difficult to corrode than the η-Zn phase.[41] From the results mentioned above, in the plated films obtained from the IME-containing solution, the dissolution reaction of plated films seems to be suppressed due to an increase in the γ-phase.

4.2. Corrosion Resistance after the Formation of Corrosion Products with 48 Hours of Immersion in NaCl Solution

The corrosion current density of Zn–Ni alloy-plated films after the formation of corrosion products with 48 hours of immersion in 3 mass% NaCl solution was evidently smaller with the addition of IME to the plating solution (Fig. 8). The schematic diagram of the inner polarization curve of the Zn–Ni alloy-plated films considered from Fig. 8 is shown in **Fig. 14**. The decrease in corrosion current density with the addition of IME in the plating solution is caused by the suppression of the reduction reaction of dissolved oxygen. The anode reaction of the Zn–Ni alloy-plated films with corrosion products (dissolution reaction of plated films) was more significantly suppressed with the addition of IME to the plating solution. As a result, the corrosion potential largely shifted toward the noble direction with the addition of IME to the plating solution.

With IME added to the plating solution, the surface morphology of the Zn chloride hydroxide ($ZnCl_2 \cdot 4Zn(OH)_2$) of the corrosion product changed. Zn chloride hydroxide was uniformly formed on the surface with an increasing concentration of IME (Figs. 9, 12). The reason why the reduction reaction of dissolved oxygen and the dissolution reaction of the plated films obtained from IME-containing solutions was suppressed is attributed to the Zn chloride

hydroxide of the corrosion product being uniformly formed on the surface.

To evaluate the amount of C co-deposited, the Zn–Ni alloy-plated films obtained at 500 $A \cdot m^{-2}$ and 5×10^4 $C \cdot m^{-2}$ on a Cu substrate were analyzed with rf-GDOES. The result is shown in **Fig. 15**. In Zn–Ni alloy-plated films obtained from the IME-free solution (Fig. 15(a)), C was co-deposited in the plated films, which is attributed to the triethanolamine added as a complex agent with Ni^{2+} ions. The C content in plated films obtained from the IME-containing solutions were evidently higher than that without IME (Figs. 15(b), 15(c)), indicating the co-deposition of a component of the IME.

The reason why the corrosion products in the Zn–Ni alloy-plated films obtained from the IME-containing solutions were uniformly formed on the surface was thought to be because the surface of the plated films became smooth with the addition of IME (Fig. 2), the anode reaction (dissolution reaction of plated films) was suppressed due to an increase in the γ-phase in the plated films and the co-deposition of a component of the IME, but details are unknown.

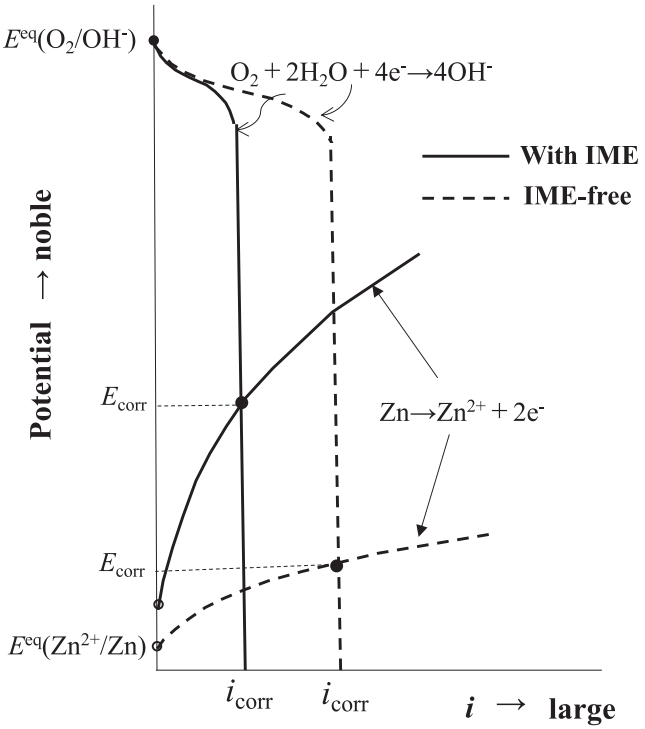

Fig. 14. Schematic diagram of internal polarization curves after the formation of corrosion products on deposits obtained in the solutions with and without IME.

5. Conclusion

The corrosion resistance of Zn–Ni alloy-plated films obtained from the solution containing the reaction product of epichlorohydrin and imidazole (IME) was evaluated using the polarization curve in 3 mass% NaCl solution. Immediately after the formation of the plated films, the reduction reaction of dissolved oxygen rarely changed regardless of whether IME was added to the zincate solution. As a result, the effect of IME on the corrosion current density of the plated films was not observed. However, in films plated from the solution containing IME, the anode reaction or dissolution reaction of films was suppressed, resulting in a shift toward the noble direction of the corrosion potential. With increasing concentrations of IME in the plating solution, the degree of anode reaction suppression and the shift of corrosion potential toward the noble direction increased. The suppression of the dissolution reaction of the plated films with the addition of IME is attributed to the increase in the γ-phase within the plated films.

After the formation of corrosion products on plated films obtained from IME-containing solutions with 48 hours of immersion in 3 mass% NaCl solution, the reduction reaction of dissolved oxygen was suppressed with increasing concentrations of IME in the plating solution, resulting in a decrease in corrosion current density. With increasing concentrations of IME added to the plating solution, the surface morphology of the Zn chloride hydroxide ($ZnCl_2 \cdot 4Zn(OH)_2$) of the corrosion products changed and Zn chloride hydroxide was uniformly formed on the surface. This seemed to cause the suppression of the reduction reaction of dissolved oxygen.

REFERENCES

1) R. Ramanauskas: *Appl. Surf. Sci.*, **153** (1999), 53. https://doi.org/10.1016/S0169-4332(99)00334-7
2) Z. Feng, Q. Li, J. Zhang, P. Yang, H. Song and M. An: *Surf. Coat. Technol.*, **270** (2015), 47. https://doi.org/10.1016/j.surfcoat.2015.03.020

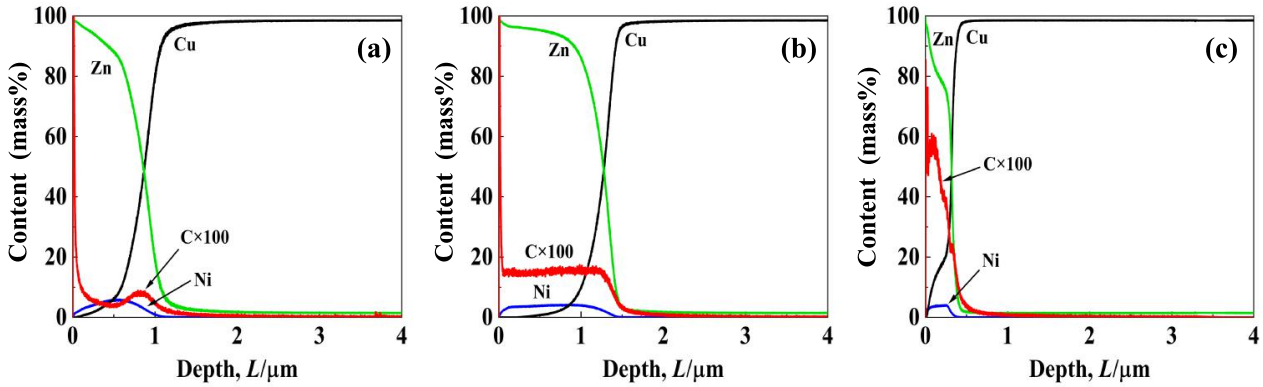

Fig. 15. Rf-GDOES depth profiles of films deposited at 500 $A \cdot m^{-2}$ and 5×10^4 $C \cdot m^{-2}$ in solutions containing various amounts of IME. [(a) IME-free, (b) IME 1 $mL \cdot dm^{-3}$, (c) IME 3 $mL \cdot dm^{-3}$, (d) IME 5 $mL \cdot dm^{-3}$]. (Online version in color.)

3) S. H. Mosavat, M. H. Shariat and M. E. Bahrololoom: *Corros. Sci.*, **59** (2012), 81. https://doi.org/10.1016/j.corsci.2012.02.012
4) O. Girčienė, L. Gudavičiūtė, R. Juškėnas and R. Ramanauskas: *Surf. Coat. Technol.*, **203** (2009), 3072. https://doi.org/10.1016/j.surfcoat.2009.03.030
5) H. Nakano, M. Matsuno, S. Oue, M. Yano, S. Kobayashi and H. Fukushima: *Mater. Trans.*, **45** (2004), 3130. https://doi.org/10.2320/matertrans.45.3130
6) A. El Hajjami, M. P. Gigandet, M. De Petris-Wery, J. C. Catonne, J. J. Duprat, L. Thiery, F. Raulin, N. Pommier, B. Starck and P. Remy: *Appl. Surf. Sci.*, **254** (2007), 480. https://doi.org/10.1016/j.apsusc.2007.06.016
7) H. Nakano, S. Kobayashi, T. Akiyama, T. Tsuru and H. Fukushima: *Tetsu-to-Hagané*, **89** (2003), 64 (in Japanese). https://doi.org/10.2355/tetsutohagane1955.89.1_64
8) H. Nakano, M. Matsuno, S. Oue, M. Yano, S. Kobayashi and H. Fukushima: *J. Jpn. Inst. Met. Mater.*, **69** (2005), 548 (in Japanese). https://doi.org/10.2320/jinstmet.69.548
9) V. Narasimhamurthy and L. H. Shivashankarappa: *J. Adv. Electrochem.*, **6** (2020), 188. https://doi.org/10.30799/jaec.061.20060103
10) S. Anwar, Y. Zhang and F. Khan: *RSC Adv.*, **8** (2018), 28861. https://doi.org/10.1039/c8ra04650f
11) C. Cachet, B. Saïdani and R. Wiart: *J. Electrochem. Soc.*, **138** (1991), 678. https://doi.org/10.1149/1.2085657
12) A. Abibsi, J. K. Dennis and N. R. Short: *Trans. IMF*, **69** (1991), 145. https://doi.org/10.1080/00202967.1991.11870911
13) M. G. Hosseini, H. Ashassi-Sorkhabi and H. A. Y. Ghiasvand: *Surf. Coat. Technol.*, **202** (2008), 2897. https://doi.org/10.1016/j.surfcoat.2007.10.022
14) H. Nakano, S. Arakawa, Y. Takada, S. Oue and S. Kobayashi: *Mater. Trans.*, **53** (2012), 1946. https://doi.org/10.2320/matertrans.M2012241
15) H. Nakano, S. Arakawa, Y. Takada, S. Oue and S. Kobayashi: *J. Jpn. Inst. Met. Mater.*, **76** (2012), 443 (in Japanese). https://doi.org/10.2320/jinstmet.76.443
16) S. H. Bae, S. Oue, Y.-k. Taninouchi, I. Son and H. Nakano: *Tetsu-to-Hagané*, **108** (2022), 120 (in Japanese). https://doi.org/10.2355/tetsutohagane.TETSU-2021-092
17) S. H. Bae, S. Oue, Y.-k. Taninouchi, I. Son and H. Nakano: *ISIJ Int.*, **62** (2022), 1522. https://doi.org/10.2355/isijinternational.ISIJINT-2022-076
18) H. Nakano, S. Arakawa, S. Oue and S. Kobayashi: *Tetsu-to-Hagané*, **99** (2013), 425 (in Japanese). https://doi.org/10.2355/tetsutohagane.99.425
19) H. Nakano, S. Shibata, S. Arakawa, S. Oue and S. Kobayashi: *ISIJ Int.*, **53** (2013), 1858. https://doi.org/10.2355/isijinternational.53.1858
20) Z. Feng, Q. Li, J. Zhang, P. Yang and M. An: *RSC Adv.*, **5** (2015), 58199. https://doi.org/10.1039/C5RA09582D
21) G. Y. Li, J. S. Lian, L. Y. Niu and Z. H. Jiang: *Surf. Coat. Technol.*, **191** (2005), 59. https://doi.org/10.1016/j.surfcoat.2004.04.062
22) S. H. Mosavat, M. E. Bahrololoom and M. H. Shariat: *Appl. Surf. Sci.*, **257** (2011), 8311. https://doi.org/10.1016/j.apsusc.2011.03.017
23) J. S. Kavirajwar, B. Shivarudraiah and Y. Arthoba Nayaka: *J. Electrochem. Sci. Eng.*, **9** (2019), No. 3, 175. https://doi.org/10.5599/jese.606
24) L. M. Muresan, J. Eymard, D. Blejan and E. Indrea: *Stud. Univ. Babes-Bolyai Chem.*, **55** (2010), No. 1, 37. https://www.researchgate.net/publication/235654567, (accessed 2010-01-01).
25) J. S. Kavirajwar and S. Basavanna: *Int. J. Appl. Eng. Manag. Lett.*, **4** (2020), 51. https://doi.org/10.5281/zenodo.3773923
26) Z. Feng, L. Ren, J. Zhang, P. Yang and M. An: *RSC Adv.*, **6** (2016), 88469. https://doi.org/10.1039/C6RA18476F
27) H. Hagi and H. Yotsugi: *J. Surf. Finish. Soc. Jpn.*, **48** (1997), 206 (in Japanese). https://doi.org/10.4139/sfj.48.206
28) H. Hagi, T. Nagata and Y. Hayashi: *J. Surf. Finish. Soc. Jpn.*, **40** (1989), 1126 (in Japanese). https://doi.org/10.4139/sfj.40.1126
29) Y. Miyoshi, J. Oka and S. Maeda: *Trans. Iron Steel Inst. Jpn.*, **23** (1983), 974. https://doi.org/10.2355/isijinternational1966.23.974
30) S. H. Bae, S. Oue, Y.-k. Taninouchi, I. Son and H. Nakano: *ISIJ Int.*, **62** (2022), 1918. https://doi.org/10.2355/isijinternational.ISIJINT-2022-160
31) S. H. Bae, S. Oue, Y.-k. Taninouchi, I. Son and H. Nakano: *Tetsu-to-Hagané*, **108** (2022), 268 (in Japanese). https://doi.org/10.2355/tetsutohagane.TETSU-2021-105
32) S. H. Bae, S. Oue, I. Son and H. Nakano: *ISIJ Int.*, **61** (2021), 2256. https://doi.org/10.2355/isijinternational.ISIJINT-2021-080
33) S. Bae, S. Oue, I. Son and H. Nakano: *Tetsu-to-Hagané*, **107** (2021), 229 (in Japanese). https://doi.org/10.2355/tetsutohagane.TETSU-2020-108
34) H. Nezu, S. Fujii, N. Kaneko and M. Ofuchi: *J. Met. Finish. Soc. Jpn.*, **32** (1981), 17 (in Japanese). https://doi.org/10.4139/sfj1950.32.17
35) S. Konishi, S. Eguchi, N. Ozeki and M. Uesugi: *J. Met. Finish. Soc. Jpn.*, **20** (1969), 263 (in Japanese). https://doi.org/10.4139/sfj1950.20.263
36) T. Iwai: *Zairyo-to-Kankyo*, **42** (1993), 236. https://doi.org/10.3323/jcorr1991.42.236
37) A. Komatsu, H. Izutani, T. Tsujimura, A. Andoh and T. Kittaka: *Tetsu-to-Hagané*, **86** (2000), 534 (in Japanese). https://doi.org/10.2355/tetsutohagane1955.86.8_534
38) M. Hansen: Constitution of Binary Alloys, McGraw-Hill Book, New York, (1958), 1060.
39) S. Haruyama: Hyomen Gijutsusha no tameno Denkikagaku (Electrochemistry for Surface Engineer), Maruzen, Tokyo, (2005), 155 (in Japanese).
40) S. Haruyama: Hyomen Gijutsusha no tameno Denkikagaku (Electrochemistry for Surface Engineer), Maruzen, Tokyo, (2005), 178 (in Japanese).
41) A. Shibuya, T. Kurimoto, K. Korekawa and K. Noji: *Tetsu-to-Hagané*, **66** (1980), 771 (in Japanese). https://doi.org/10.2355/tetsutohagane1955.66.7_771